

Small Methods

Unsupervised learning for the segmentation of small crystalline particles at the atomic level

--Manuscript Draft--

Manuscript Number:	smtd.202201175
Article Type:	Research Article
Corresponding Author:	Arturo Ponce-Pedraza, Ph.D. The University of Texas at San Antonio San Antonio, Texas UNITED STATES
Corresponding Author E-Mail:	arturo.ponce@utsa.edu
Order of Authors:	Arturo Ponce-Pedraza, Ph.D. Guillermo Bárcena-González Andrei Hernández-Robles Álvaro Mayoral Lidia Martinez Yves Huttel Pedro L. Galindo
Keywords:	Unsupervised learning; Gabor filters; crystal orientation mapping; large datasets
Manuscript Classifications:	SYSTEMS & MODELING - complex systems, theory, simulations, modeling, computational methods, artificial intelligence, machine learning, neural networks
Section/Category:	
Abstract:	<p>Electron backscattering diffraction provides the analysis of crystalline phases at large scales (microns) while precession electron diffraction may be used to get 4D-STEM data to elucidate structure at nanometric resolution. Both are limited by the probe size and also exhibit some difficulties for the generation of large datasets, given the inherent complexity of image acquisition. The latter appoints the application of advanced machine learning techniques, such as deep learning adapted for several tasks, including pattern matching, image segmentation, etc.</p> <p>This research aims to show how Gabor filters provide an appropriate feature extraction technique for electron microscopy images that could prevent the need of large volumes of data to train deep learning models. The work herein presented combines an algorithm based on Gabor filters for feature extraction and an unsupervised learning method to perform particle segmentation of polyhedral metallic nanoparticles and crystal orientation mapping at atomic scale.</p> <p>Experimental results have shown that Gabor filters are convenient for electron microscopy images analysis, that even a non-supervised learning algorithm can provide remarkable results in crystal segmentation of individual nanoparticles. This approach enables its application to dynamic analysis of particle transformation recorded with aberration-corrected microscopy, offering new possibilities of analysis at nanometric scale.</p>
Suggested Reviewers:	<p>Sandra Van Aert University of Antwerp: Universiteit Antwerpen sandra.vanaert@uantwerpen.be</p> <p>Eric Stach University of Pennsylvania stach@seas.upenn.edu</p> <p>Jordi Arbiol Institut Català de Nanociència i Nanotecnologia: Institut Catala de Nanociencia i Nanotecnologia jordi.arbiol@icn2.cat</p>

Unsupervised learning for the segmentation of small crystalline particles at the atomic level

*Guillermo Bárcena-González, Andrei Hernández-Robles, Álvaro Mayoral, Lidia Martinez, Yves Huttel, Pedro L. Galindo, Arturo Ponce**

A. Hernandez-Robles, A. Ponce

Department of Physics and Astronomy, University of Texas at San Antonio, San Antonio, Texas 78249, USA.

E-mail: arturo.ponce@utsa.edu

G. Bárcena-González, P.L Galindo

Department of Computer Engineering, ESI, University of Cádiz, Puerto Real 11510, Spain

A. Mayoral

Instituto de Nanociencia y Materiales de Aragón (INMA), CSIC-Universidad de Zaragoza, Zaragoza 50009, Spain.

Advanced Microscopy Laboratory (LMA), University of Zaragoza, 50018, Zaragoza Spain.

L. Martinez, Y. Huttel

Instituto de Ciencia de Materiales de Madrid (ICMM-CSIC), 28049, Madrid, Spain.

Keywords: Unsupervised learning, Gabor filters, crystal orientation mapping, large datasets

Electron backscattering diffraction provides the analysis of crystalline phases at large scales (microns) while precession electron diffraction may be used to get 4D-STEM data to elucidate structure at nanometric resolution. Both are limited by the probe size and also exhibit some difficulties for the generation of large datasets, given the inherent complexity of image acquisition. The latter appoints the application of advanced machine learning techniques, such as deep learning adapted for several tasks, including pattern matching, image segmentation, etc. This research aims to show how Gabor filters provide an appropriate feature extraction technique for electron microscopy images that could prevent the need of large volumes of data to train deep

learning models. The work herein presented combines an algorithm based on Gabor filters for feature extraction and an unsupervised learning method to perform particle segmentation of polyhedral metallic nanoparticles and crystal orientation mapping at atomic scale.

Experimental results have shown that Gabor filters are convenient for electron microscopy images analysis, that even a non-supervised learning algorithm can provide remarkable results in crystal segmentation of individual nanoparticles.

This approach enables its application to dynamic analysis of particle transformation recorded with aberration-corrected microscopy, offering new possibilities of analysis at nanometric scale.

1. Introduction

Properties of nanomaterials are governed by both intrinsic and extrinsic factors, they typically undergo a nanometric revamp process of the regular patterns expected from their bulk crystalline models, for instance, propitiating the appearance of a broad type of defects that can be categorized by their grain size and crystal orientation.^[1] Consequently, it is critical to obtain the crystallographic profile to correlate physical properties to the nanometric structures. Historically, transmission electron microscopy (TEM) methods have been employed to retrieve atomic resolution images, especially since the development and implementation of aberration correctors, scanning-TEM (STEM), and high-angle annular dark-field imaging (HAADF). Additionally, electron diffraction has been extensively used as a complementary technique to elucidate crystallographic information from materials under various modalities such as selected area electron diffraction, microdiffraction, nanobeam diffraction (NBD) or convergent beam electron diffraction (CBED) and electron backscattering diffraction (EBSD).^[2] Besides, coupled with STEM, electron diffraction can also be collected while the beam continuously scans the sample using precession electron diffraction (PED) coupled with one of the abovementioned detectors can lead to get 4D-STEM data which have been recently developed to elucidate structure at smaller scales, but further development needs to be done in the collection and analysis of big data.^[3] EBSD provides the analysis of crystalline phases, strain, and crystal orientation mapping at larger scale (microns), while PED-based method produces similar maps but reaching nanometric resolution, both methodologies are limited by the probe size, one can classify the ranges of the analyzed area in squared microns and nanometers, respectively. In both electron diffraction scanning methods, EBSD and PED, the manipulation of large datasets is crucial due

to the fast electron diffraction acquisition and pattern matching. The aim of both methods is the collection of crystal orientation and phase maps with high reliability and to acquire them in short periods preventing damaging specimens in the process.^[4–7]

Consequently, computational methods have been developed for the analysis of HRTEM images and electron diffraction patterns, including methods oriented towards particle segmentation, that have been adapted to use image processing algorithms based on supervised and unsupervised learning methods.^[8–12] Particle segmentation has been divided mainly into two sectors: tracing the particle shape and size, and crystal orientation mapping.^[13,14] These techniques have been further developed using learning-based methods that often need large training datasets with specific parameters to carry out their functions. Despite this fact, the use of classical computer vision-based algorithms can be implemented for electron microscopy analysis to avoid the collection and processing of large volumes of data to train these models. The work herein presented combines an algorithm based on Gabor filters to perform particle segmentation of polyhedral metallic nanoparticles and crystal orientation mapping at atomic scale, leading to perform the same tasks in a different scale without using experimental techniques or learn-based models. The importance of our findings is not only the reliability of crystal segmentation at individual nanoparticles but the possibility to extend the application into dynamic analysis of particle transformation recorded with aberration-corrected microscopy, opening new possibilities of analysis at nanometric scale.

1.1 Gabor filters

Dennis Gabor, Nobel laureate in physics in 1971, pioneered in the field of phase retrieval methods in electron optics by inventing electron holography.^[15] Since then, electron holography methods have evolved into phase retrieval being able to reach sub-nanometric resolution using HRTEM imaging. The retrieved phase from electron micrographs contains physical information from the sample due to the phase shift affected by intrinsic electrostatic and magnetostatic potentials, and strain, normally evaluated by Fourier space analysis.^[16–21]

In his work, Dennis Gabor showed that the uncertainty principle also applies to signals, as a signal cannot simultaneously be localized in both frequency and time domains, that is, there exists a trade-off between time resolution and frequency resolution, and there is a lower bound on their joint product.^[22] Gabor demonstrated that the product of a Gaussian-shaped kernel

(known as the envelope) times a complex sinusoid (known as the carrier) is the most general function to obtain the minimum of the uncertainty principle, thus yielding the maximal accuracy in the time-frequency-scale combined space.^[23] A Gabor filter is a linear filter based on this idea, and it was originally developed for 1D signal analysis. Daugman extended the Gabor filter to two dimensions (2D) and, since then, it has been found to be particularly appropriate for texture analysis, feature extraction, edge detection, image compression and a multitude of image-related fields^[22,24–28] These filters are commonly described as a function produced by a Gaussian-shaped kernel times a complex sinusoid. In a spatial domain, a 2D Gabor filter is defined as a Gaussian kernel function (w) modulated by a complex sinusoidal plane wave(s):

$$g(x, y) = w(x, y) * s(x, y) \quad (1)$$

$$w(x, y) = \frac{1}{\sqrt{2\pi}\sigma} e^{-\frac{1}{2}\left(\frac{x^2}{\sigma_x^2} + \frac{y^2}{\sigma_y^2}\right)} \quad (2)$$

$$s(x, y) = e^{-2\pi i(u_0 x + v_0 y + \varphi)} \quad (3)$$

where σ is the standard deviation of the gaussian, σ_x^2 and σ_y^2 are the variance in x-axis and y-axis and determines the width of the major and minor axis of the Gaussian envelope. On the other hand, u_0, v_0 parameters define the spatial frequency of the sinusoid and φ defines its phase. As a Gabor filter is the product of a Gaussian and a sinusoid, its Fourier transform is the convolution of its transforms, that is, a Gaussian centered in the harmonic function frequency associated to the sinusoidal. This property is essential to understand why Gabor filters are so efficient at extracting features depending on its fringe orientation and spacing, making Gabor filtering a very useful tool for the analysis of electron microscopy images of crystalline materials. Simplifying the product of functions in (1), the Gabor filter can be defined as:

$$g(x, y, \sigma_x, \sigma_y, \theta, \gamma, \lambda, \varphi) = e^{-\frac{1}{2}\left(\frac{x'^2}{\sigma_x^2} + \frac{y'^2 \gamma^2}{\sigma_y^2}\right)} e^{i\left(2\pi \frac{x'}{\lambda} + \varphi\right)} \quad (4)$$

Where

$$x' = x \cos(\theta) + y \sin(\theta) \quad (5)$$

$$y' = -x \sin(\theta) + y \cos(\theta) \quad (6)$$

The most important parameters of a Gabor filter are the orientation angle (θ) and the wavelength (λ), the latter parameter is just the spacing between fringes, and therefore, the filtering channel.

The effect of the variation of the wavelength variable is observed in Figure S1 a-c, where λ is proportional to the width of the filter channel. while the change in orientation of a Gabor filter can be visualized in Figure S1. d-f.

Gabor filtering of an image $f(x,y)$ is obtained as its convolution with the Gabor filter

$f_g(x, y, \sigma_x, \sigma_y, \theta, \gamma, \lambda, \varphi)$:

$$f_g(x, y, \sigma_x, \sigma_y, \theta, \gamma, \lambda, \varphi) = f(x, y) * g(x, y, \sigma_x, \sigma_y, \theta, \gamma, \lambda, \varphi) \quad (7)$$

Gabor filtering highlights the local texture with the same orientation and wavelength as the applied filter. By varying the orientation, features oriented in a particular direction are passed. In a similar way, by varying the wavelength, textures containing fringe patterns at different spacing are highlighted. Furthermore, (σ_x, σ_y) parameters allow controlling the 2D filter bandwidth, that is, the size of the image region contributing a given pixel value in the filtered image. In order to extract relevant features from an image, a Gabor filter-bank may be designed, consisting of a set of Gabor filters with different orientations and spacings (usually covering all space and orientation). The output of this filter-bank may be used to characterize each pixel of the original image based on the fringe patterns present in its surroundings.

1.1.1. Feature extraction using Gabor filters

To understand the power of feature extraction of Gabor filters, the FFT analysis of a micrograph is reviewed. It starts with the calculation of the FFT of a region of interest (ROI) in the particle to be segmented as shown in in **Figure 1** (a). A spot pattern is acquired such as the one displayed in the inset of Figure 1 (a). An atomic model of the associated decahedral particle oriented along the five-fold symmetry is shown in Figure 1 (b), which is perpendicular to the electron beam direction. Thus, the five tetrahedra that forms the pentagonal particle are oriented along the [110]

direction. By selecting a specific reflection (red circle in the inset Fig 1 (a)), and applying a Bragg filter to the whole image yields a strong response on the atomic) planes having a specific orientation and wavelength, as shown in the Bragg image of Figure 1 (c). On the other hand, if we design a Gabor filter with the orientation and wavelength associated to the chosen Bragg spot and apply this filter to the whole image, yields a response image where the pixels corresponding to the same area are clearly highlighted, as shown in Figure 1 (d).

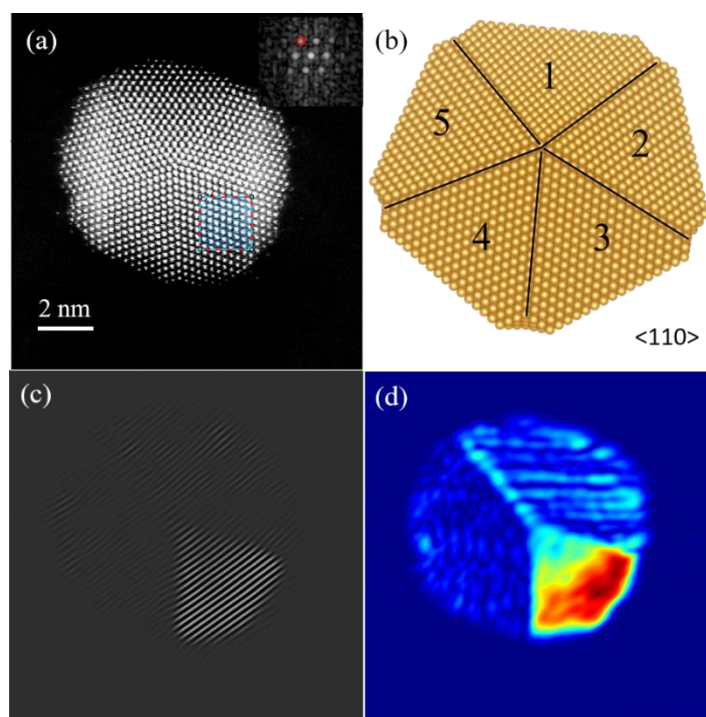


Figure 1. Illustrative sequence showing the feature extraction power of a single Gabor filter. (a) Experimental C_s -corrected STEM HAADF image of an Au decahedron. The dashed rectangle indicates the ROI where the FFT diffractogram (inset) was extracted from. An FFT of a selected region is applied, the inset image represents the FFT taken from the ROI, a selected reflection is marked by a red circle in the inset to select a specific family of crystal planes and get orientations and wavelength. (b) Geometrical model of the pentagonal nanoparticle target. (c) Bragg image of the selected reflection highlighting the selected spot plane. (d) Response image after applying the Gabor filter with the estimated features yielding a response image where the observation is evidenced.

Nanoparticles studied under HRTEM conditions produce images particularly suited for fast Fourier transforms (FFTs) analysis, for most of these structures crystalline order will be

predominant in the specimen, producing typical spot pattern diffractograms. However, the obtention of FFTs at specific facets or defects of geometrical shaped nanoparticles considerably reduces the definition of the produced FFT image. This is because conventional software is not suited to retrieve proper Fourier diffractograms of small areas (as those present in small nanoparticles). However, Gabor filters provide a local response, only restricted by the resolution of the image, which for state-of-the-art microscopes, is translated to sub-angstrom resolution, avoiding the use of external devices that retrieves diffraction patterns that often sacrifices resolution due the nature of the techniques such as PED.

In this work, we propose the use of a bank of Gabor filters for feature extraction and the use of unsupervised learning for image segmentation and crystal orientation mapping at atomic resolution.

2. Results and discussions

The first specimens were studied using STEM data, **Figure 2** (a). contains two nanostructures: a decahedral nanoparticle (inside the red-dotted square) and an icosahedral nanoparticle (yellow-dotted square), both of about 7 nm in diameter. By following the above-described procedure, the segmentation of the decahedral particle detects the expected five facets and the background for $k = 6$. The resultant segmentation of the nanoparticle is consistent with the pentagonal particle, the k value converges as $k = n + 1$. On the other hand, the icosahedral particle in the same image is oriented in a direction such that 7 ($n = 7$) twins are projected. Color maps of the segmentation in both particles are shown in Figures 3 (c) and (e) respectively, however, these are not oriented in a specific order.

Due to the strong contrast produced in STEM-HAADF data, this kind of images are more suitable to be used with the Gabor filters. Nevertheless, as large datasets (especially for in-situ experiments) are produced in TEM mode, the applicability of this methodology was also investigated for HRTEM images. The analysis of the Cs-corrected HRTEM image of a decahedral particle is shown in Figure S2, despite the vitiated conditions produced by the background noise, the algorithm managed to optimally discern the facets present in the particle.

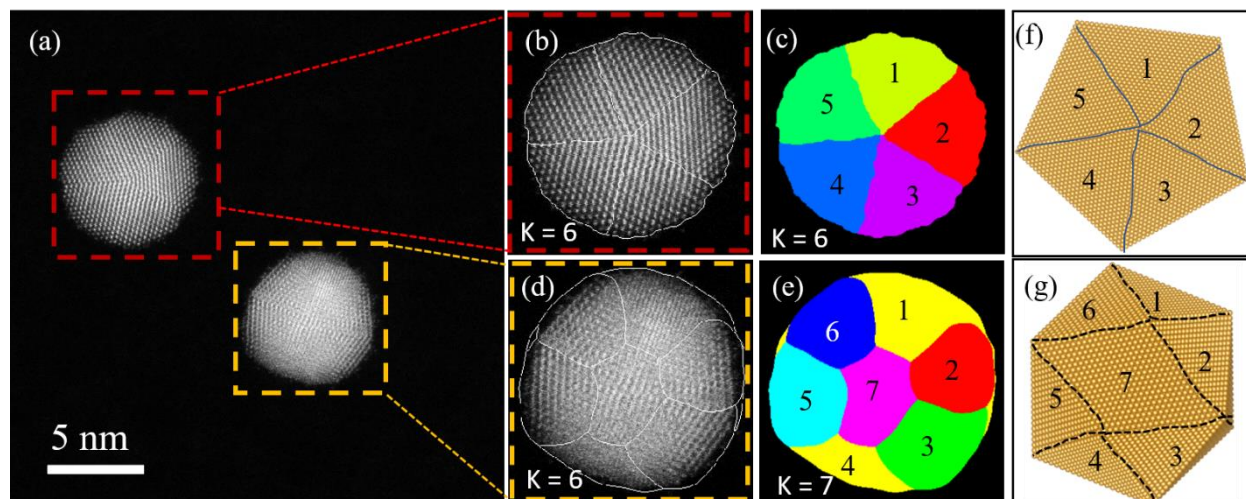


Figure 2. Particle segmentation of two particles. (a) Complete field of view of the micrograph. (b) skeletonization of the measured observations ($K=6$). (c) cluster coloring of (b). (d) delimitation of facets of icosahedral particle near the two-fold axis orientation ($K=7$). (e) segmentation after applying the coloring of the detected observations.

It is noticeable that by increasing the k values the number of segments remains unaltered; however, artifacts start to be visible, those artifacts are related to regions in which the background has a similar contrast with the nanoparticles or showing edge unfocused regions. The set of C_s -corrected HRTEM images shown in **Figure 3** includes two multi-twinned nanoparticles (yellow and red dashed squares) and another one that correspond to a single *fcc* nanoparticle (blue dashed square) oriented along the $[110]$ direction that were segmented under our method. Despite the subtle contrast difference between, the result is consistent with the evident number of twins projected in the C_s -HRTEM images, for twinned particles the k value converges at 2 (Figures 3 (e) and (f)) and the *fcc* nanoparticle at 1 (Figure 3 (g)).

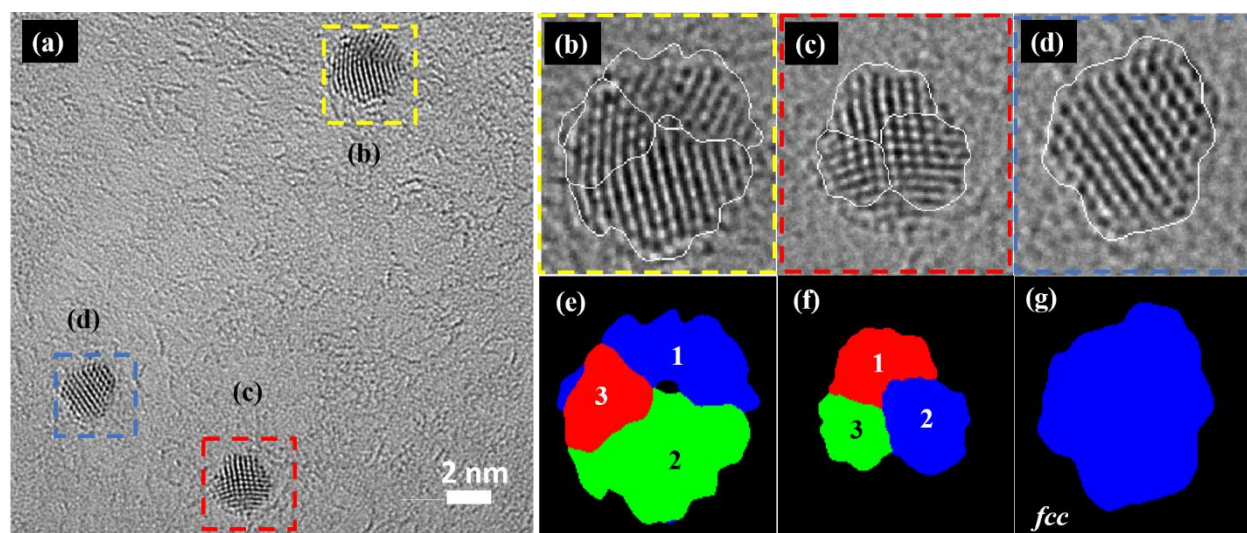


Figure 3. Segmentation of multiple metallic clusters. (a) Complete C_s -HRTEM image, the three metallic cluster are indicated by dotted squares. (b)-(d) Segmentation of each individual cluster. (e) and (f) Color maps of the multiple twinned clusters (b) and (c). (g) Color map of the single *fcc* cluster.

To evaluate the viability of the method on more complicated systems, a set of small clusters and coalesced nanoparticles has been analyzed, where k value was increased sequentially, the sequence is shown in **Figure 4** and **Figure S3**. The C_s -corrected STEM-HAADF image, Figure 4 (a), consists of two cojoined decahedral particles, in which the Gabor-based algorithm reaches convergence for $k = 8$. For this k -value the central particle displays 9 identified twins, some of them sharing attributes marked in Figure 6c' in same colors (6 and 3 at the main particle; 3 at the left top corner particle, and 2 in the main particle and the small section between 5 and 6 in the main particle). Additionally, for the twinned particle found in the left corner of the image one clear twin is identified (2 & 3) and an additional lattice inclusion was detected in section marked as 1. The larger k values the more features are visualized; however, the correct segments remain unaltered. Isolated particles in which the periodicity of the lattice is found is also identified at lower k values and enhanced at larger k values. The whole sequence from $k = 2$ to $k = 16$ is shown in **Figure S3** of the supplementary information as a demonstration of no sub-segmentations of the main features.

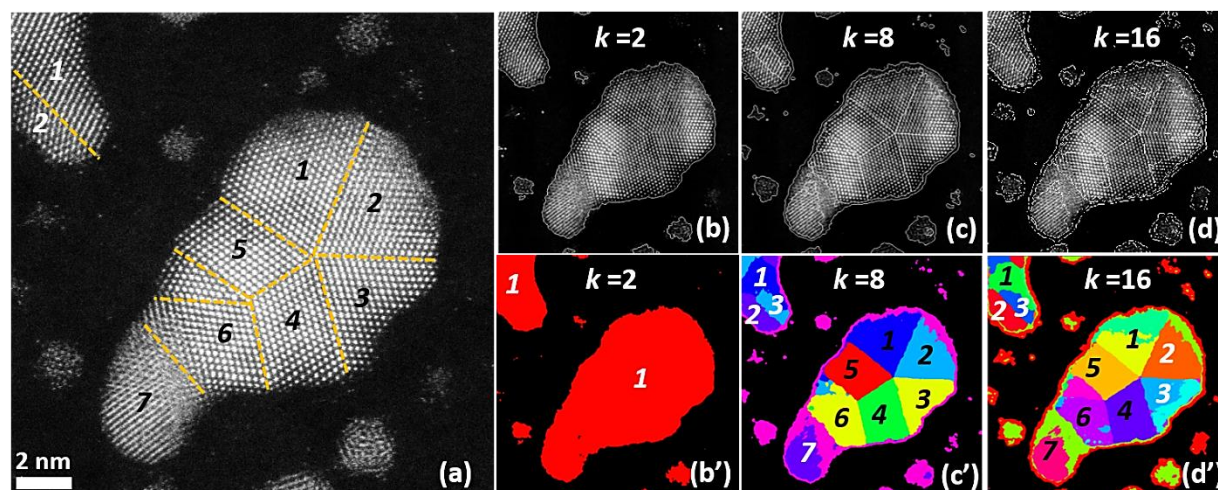


Figure 4. A sequence of k values is shown in the multiple twinned nanoparticles and isolated small clusters and colorization: (a) Complete Cs-HRTEM image, indicating the twins of the particles. Segmentation and color maps for (b) $k = 2$; (c) $k = 8$; (d) and $k = 16$. Number of crystalline entities within the particles are indicated.

Similarly, the algorithm was tested with a set of simulated images. A gold decahedron particle of ~22000 particles (~ 13.1 nm in diameter) oriented at the five-fold axis was simulated using QSTEM^[29] along a ~2nm thick amorphous carbon layer reproducing the setup of the systems used to image in TEM. **Figure 5** represents the results of the images obtained in QSTEM, Figure 5 (a) & (b) represent images taken by a bright field (BF) detector (5-40 mrad) in STEM mode, mimicking image conditions closer to those taken in a typical HRTEM image. In contrast, HAADF image (15-150 mrad) was projected in d & e. For both systems, the clustering process converged at $k=6$ as their experimental images counterparts and despite the noise induced by the amorphous carbon layer (visible in both images) it was read as part of the “void” background, this can be observed in the ground truth images included for each system in (c) and (f).

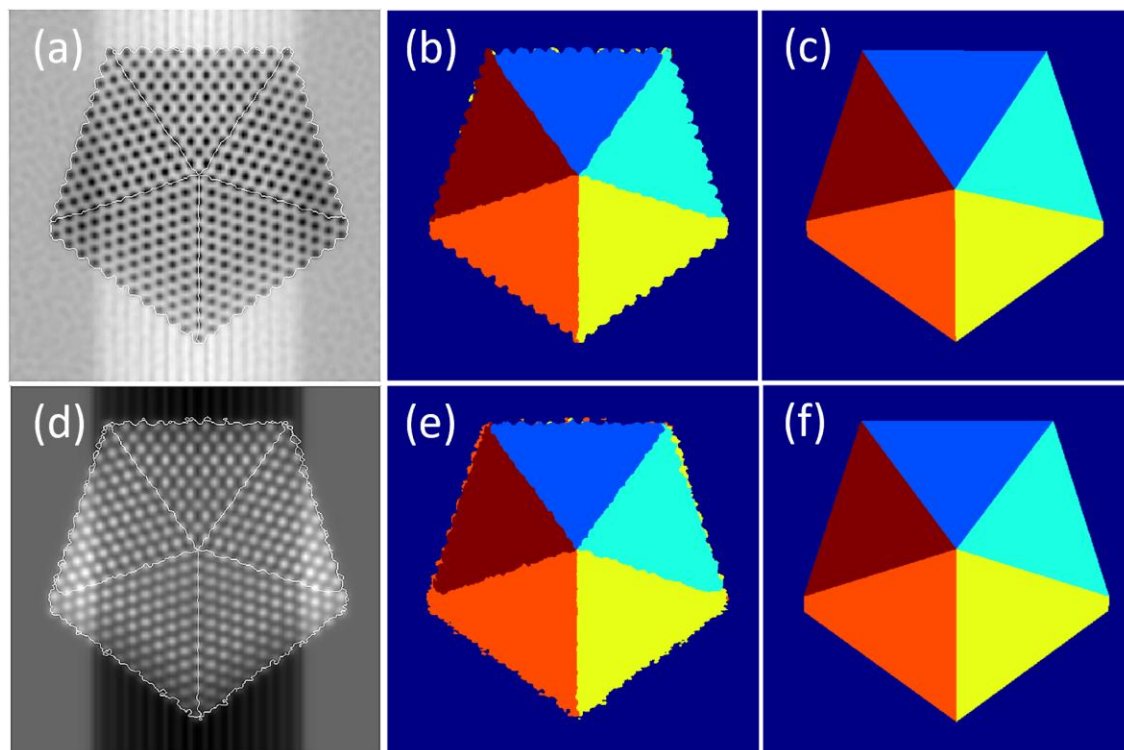


Figure 5. Segmentation of simulated TEM images. (a) skeletization of the main features detected by the algorithm, the contrast difference of this BF image is low resembling an average HRTEM image. (b) Colorization of the segmentation done in (a). (c) Groundtruth of the nanoparticle in (a). (d) skeletization of the main features by the segmentation process, the contrast difference of this HAADF image is notorious as in experimental images.(e) Colorization of the segmentation done in (c). (f) Groundtruth of the nanoparticle in (d).

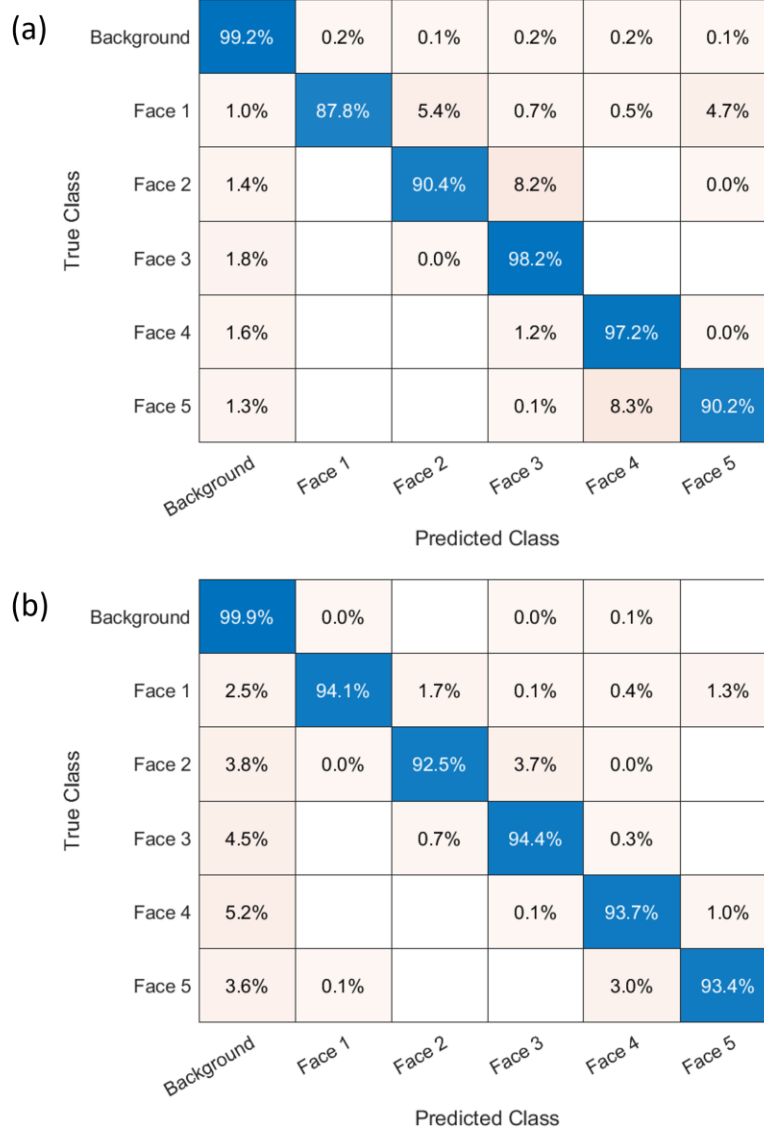


Figure 6. Percentile confusion matrices of the segmentation of the simulated images in Figure 5. a) results of the segmentation of the simulated BF image. b) results of the segmentation of the simulated DF image.

Figure 6 (a) shows the confusion matrix for Figure 5 (a). Our algorithm classifies 99.2% of the background pixels correctly, while the face pixels range from 87.8% to 98.2%. This difference is due to the fact that the atomic columns have been profiled better than the groundtruth. Even so, the accuracy reaches 96.35% and with an F1 score of 94.02%.^[30] In Figure 6 (b), corresponding to the confusion matrix of the segmentation performed for Figure 5 (d), the values are even better, with 99.9% of background pixels classified correctly, while the values for the classification of the pixels corresponding to the faces vary between 92.5% and 94.4%, with an accuracy of

96.96% and an F1 score of 95.97%. Both metrics quantitatively confirm that the proposed technique might be useful for the automatic segmentation of nanoparticle faces at the pixel level.

3. Conclusions

In conclusion, a whole methodology for the automatic segmentation of crystalline nanoparticles has been presented. It is based (i) on the application of a bank of Gabor filters as a powerful feature extraction technique for crystalline data and (ii) an unsupervised learning technique (k-means clustering) for particle segmentation. The developed algorithm allows, not only to perform the segmentation of multiple particles, but also to identify crystal orientation allowing the generation of maps in a similar fashion as in other experimental crystal orientation mapping methods based on electron diffraction, but at atomic resolution. While in this paper, a simple non-supervised learning algorithm for clustering such as *k*-means has been used for segmentation purposes, more advanced techniques based on deep learning might be applied in the future to Gabor-filtered images for more complex tasks in an automated way.

4. Methods

4.1 Production of nanoparticles

Au nanoparticles (NPs) were prepared by inert gas gas-phase condensation. In here, the different types of NPs were grown using a magnetron (Nano4Energy SL) of 2 inches in diameter, which was fitted into a standard gas aggregation source (GAS) from Oxford Applied Research Ltd.^[31–33] A stable flux of Argon was injected at the back side of the aggregation zone. The magnetron was operated at a power of 90 W and a current of 0.21 A, and the NPs were collected in an ultrahigh vacuum chamber (base pressure in the high 10^{-10} mbar) connected to the GAS. To recover the NPs for the electron microscopy observations, an ultrathin carbon coated copper TEM grid was placed at 400 mm from the exit slit of the GAS.

4.2 Electron microscopy

Spherical aberration corrected (C_s -corrected) High Angle Annular Dark Field (HAADF) Scanning Transmission Electron Microscopy (STEM) was carried out in a XFEG Titan FEI microscope operated at 300 kV, equipped with a CEOS corrector for the electron probe assuring a spatial resolution of 0.8 Å. C_s -corrected High-Resolution TEM was performed in a FEG Titan FEI microscope operated at 300 kV fitted with a corrector for the image formation system. The images used for computational methods are primarily decahedral nanoparticles ranging from 3-10 nm in diameter.

4.3 Feature Extraction

In a typical analysis, a Gabor filter bank is implemented with 36 different orientations over all space, between 0 and 180 degrees with a step of 5 degrees, and 7 different wavelengths (between 4 and 7 pixels with a step of 0.5). The latter parameter is a variable that depends on the scale and resolution of the TEM image. Applying this filter-bank to the original image generates 252 Gabor filtered complex images. It is important to note that while it is possible to decrease the step size in both the angle and wavelength parameters, refining these parameters can mislead to overloading the computational load.

4.4 Unsupervised learning

The purpose of unsupervised learning is to identify similar patterns in a dataset. For this task there are many different algorithms and no single best method for all problems.^[34,35] As we

are interested in showing the power of Gabor filter-based feature extraction for the segmentation of crystalline particles, one of the most simple and fast algorithms have been chosen, the K-means algorithm.^[36,37] K-means is an iterative process that partitions a set of observations into K groups represented by its centroid. The algorithm starts randomly selecting K centroids from the data points in the dataset, where K is equal to the number of desired clusters. Then, an iterative two-step procedure is done. In the first step, each data point is assigned to its nearest centroid. Then, in the second step, all centroids are updated to the average of all points in each cluster. The algorithm stops when the assignment of clusters does not change significantly in consecutive iterations. Another commonly used as stopping criterion is fixing a maximum number of iterations. The random initialization step causes the algorithm to be nondeterministic, so it is usual to run several initializations of the entire *k*-means algorithm and choose the cluster assignment with the lowest sum of squared errors.

The whole methodology is illustrated in **Figure 7**. The first step consists on defining the Gabor filter bank. In this study, 36 different orientations and 7 different wavelengths have been considered, so a total of $p=252$ Gabor filters is defined. When the filter bank is applied to the original image, a set of 252 images with energies dependent on the presence in the original image of atomic planes to the orientation and wavelength associated to each filter is obtained. Once all the filtered images are ready, a feature vector for each pixel position is created, consisting on the pixel value in the same position across all filtered images. Therefore, if each feature vector is a column, the feature matrix has a size of $p=252$ rows and $M \times N = 256 \times 256 = 65536$ columns, being M and N the dimensions of the image. After that, the K-means algorithm is applied to find clusters of similar patterns in the dataset.

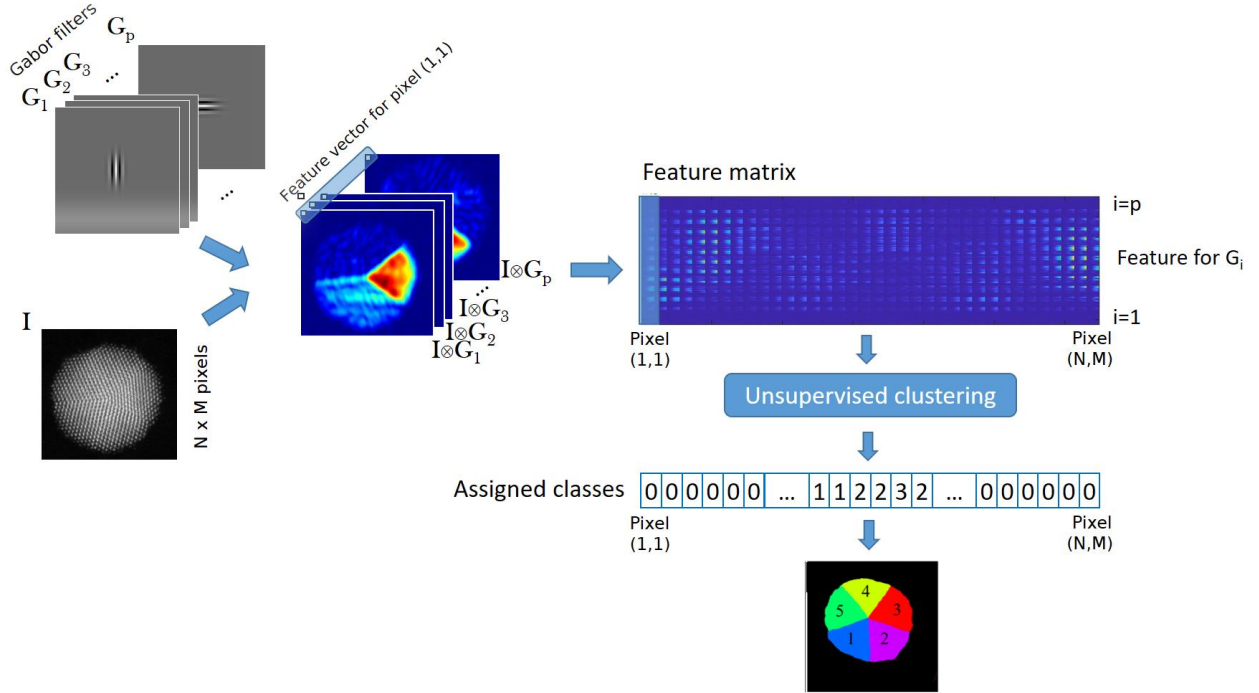


Figure 7. Diagram describing the methodology of the Gabor-filter based segmentation: (i) *Gabor filter-bank application* to get Gabor-filtered images, (ii) *Feature vector construction* for each pixel to get the Feature matrix and (iii) *Unsupervised clustering* to get assigned class for each pixel, that, rearranged back into 2D, represents the reconstruction of the segmented image.

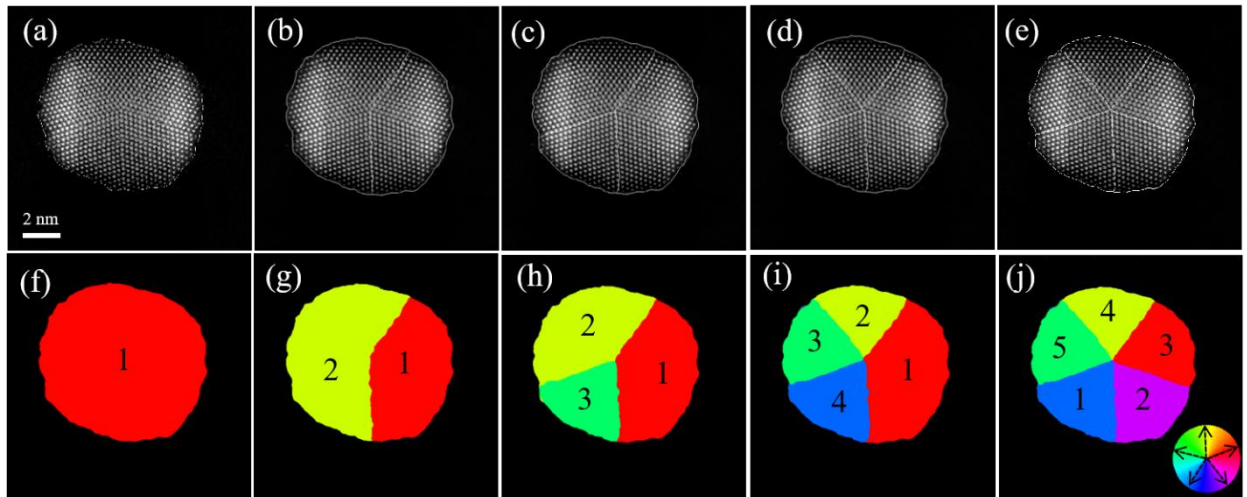


Figure 8. Sequence of a typical assignation of observations to the desired number of clusters in a TEM image displaying a decahedral nanoparticle. (a-e) $K=2-6$ respectively, where the total number of clusters correspond to the number of facets visible in the micrograph and an additional cluster that corresponds to the background. (f-j) Colorization of the assigned observations to match the different orientations and facets within the sample.

4.4.1 Dependence of the segmentation on the number of clusters

The dependence of the segmentation process as a function of K can be observed in **Figure 8 a-j)**. The sequence of the C_s -corrected STEM-HAADF image represents the detection and assignation of features to regions within the facets of the nanoparticles, the images present in the second row represent the colorization of the detected facets of the nanoparticles. Segments identified in the colored map correspond to a particular viewing direction in the pentagonal particle, Figure 8 j) includes a color wheel that matches the crystal directions, in this case it is expected a 72° rotation between each tetrahedral subunit. Note that the intermediary steps of the segmentation (Figure 8 g-i) present certain neighboring segments as part of the same cluster, this is likely due the proximity of diffraction spots in the FFT. The convergence found in the pentagonal particle is achieved by using $K=6$, as indicated in Figure 8 j). The value $K=2$ is able to discriminate the single particle and the background. Subsequently, with increasing values of K , each remaining twin of the particle is identified, until $K=6$, which indicates a total of 5 twins in the particle, plus the substrate.

Supporting Information

Supporting Information is available from the Wiley Online Library or from the author.

Conflict of interests

The author declares no conflict of interest.

Data Availability Statement

The data that support the findings of this study are available in the supplementary material of this article

Acknowledgements

AHR and GBG contributed equally to this work

AHR thanks the ConTex Doctoral Fellowship program #2019-000027-01EXTF-00125.

AM acknowledges the Spanish Ministry of Science through the Ramon y Cajal program (RYC2018-024561-I), to the regional government of Aragon (DGA E13_20R), to the European Union's Horizon 2020 research and innovation program under grant agreement No 823717 – ESTEEM3 and to the National Natural Science Foundation of China (NSFC-21835002) for funding.

Received: ((will be filled in by the editorial staff))

Revised: ((will be filled in by the editorial staff))

Published online: ((will be filled in by the editorial staff))



References


- [1] M. A. Meyers, A. Mishra, D. J. Benson, *Prog. Mater. Sci.* **2006**, *51*, 427.
- [2] X. R. Ferreres, G. Casillas, S. Aminorroaya-Yamini, A. A. Gazder, *Mater. Des.* **2020**, *185*.
- [3] C. Ophus, *Four-Dimensional Scanning Transmission Electron Microscopy (4D-STEM): From Scanning Nanodiffraction to Ptychography and Beyond*, **2019**.
- [4] E. F. Rauch, M. Véron, *Automated crystal orientation and phase mapping in TEM*, Vol. 98, Elsevier Inc., **2014**, pp. 1–9.
- [5] D. Viladot, M. Véron, M. Gemmi, F. Peiró, J. Portillo, S. Estradé, J. Mendoza, N. Llorca-Isern, S. Nicolopoulos, *J. Microsc.* **2013**, *252*, 23.
- [6] A. Ponce, J. L. Reyes-Rodríguez, E. Ortega, P. Parajuli, M. M. Hoque, A. A. Gazder, *Scanning Transmission Electron Microscopy*, Taylor and Francis group, Boca Raton, FL, USA **2020**.
- [7] A. Ponce, J. A. Aguilar, J. Tate, M. J. Yacamán, *Advances in the electron diffraction characterization of atomic clusters and nanoparticles*, RSC, **2021**, 311.
- [8] D. J. Groom, K. Yu, S. Rasouli, J. Polarinakis, A. C. Bovik, P. J. Ferreira, *Ultramicroscopy* **2018**, *194*, 25.
- [9] W. Li, K. G. Field, D. Morgan, *npj Comput. Mater.* **2018**, *4*, 1.
- [10] A. B. Oktay, A. Gurses, **2019**, *120*, 113.
- [11] K. Sytwu, C. Groschner, M. C. Scott, *Understanding the Influence of Receptive Field and Network Complexity in Neural-Network-Guided TEM Image Analysis*, arXiv, **2022**.
- [12] C. K. Groschner, C. Choi, M. C. Scott, *Microsc. Microanal.* **2021**, *27*.
- [13] J. Jeong, N. Cautaerts, G. Dehm, C. H. Liebscher, *Microsc. Microanal.* **2021**, *27*, 1102.
- [14] B. Yildirim, J. M. Cole, *J. Chem. Inf. Model.* **2021**, 1136.
- [15] D. Gabor, *Nature* **1948**, *161*, 777.
- [16] E. Snoeck, *J. Phys. D. Appl. Phys.* **2016**, *49*, 380201.
- [17] M. R. McCartney, D. J. Smith, *Annu. Rev. Mater. Res.* **2007**, *37*, 729.
- [18] A. Kovács, R. E. Dunin-Borkowski, In *Handbook of Magnetic Materials*, Elsevier, **2018**, 59.
- [19] M. I. Den Hertog, H. Schmid, D. Cooper, J. L. Rouviere, M. T. Björk, H. Riel, P. Rivallin, S. Karg, W. Riess, *Nano Lett.* **2009**, *9*.
- [20] A. Béché, J. L. Rouvière, J. P. Barnes, D. Cooper, *Ultramicroscopy* **2011**, *111*, 227.

- [21] M. J. Hytch, E. Snoeck, R. Kilaas, *Ultramicroscopy* **1998**, 74, 131.
- [22] D. Gabor, *J. Inst. Electr. Eng. - Part III Radio Commun. Eng.* **1946**, 93, 429.
- [23] A. K. Jain, F. Farrokhnia, *Pattern Recognit.* **1991**, 24, 1167.
- [24] Z. Yuanyuan, J. Xiaojun, *IASP 10 - 2010 Int. Conf. Image Anal. Signal Process.* **2010**, 656.
- [25] J. P. Jones, L. A. Palmer, *J. Neurophysiol.* **1987**, 58, 1233.
- [26] C. C. Tsai, H. Y. Lin, J. Taur, C. W. Tao, *IEEE Trans. Syst. Man, Cybern. Part B Cybern.* **2012**, 42, 150.
- [27] J. G. Daugman, *J. Opt. Soc. Am. A*, 2, **1985**, 1160.
- [28] J. G. Daugman, *Vision Res.* **1980**, 20, 847.
- [29] C. Koch, PhD thesis, Arizona State University, May, **2002**.
- [30] A. Tharwat, *Appl. Comput. Informatics* **2018**, 17, 168.
- [31] F. L. Deepak, A. Mayoral, R. Arenal, *Advanced Transmission Electron Microscopy: Applications to Nanomaterials*, Springer International Publishing AG, Switzerland, **2015**.
- [32] A. Mayoral, L. Martínez, J. M. García-Martín, I. Fernández-Martínez, M. García-Hernández, B. Galiana, C. Ballesteros, Y. Huttel, *Nanotechnology* **2019**, 30, 065606.
- [33] L. Martínez, A. Mayoral, M. Espiñeira, E. Roman, F. J. Palomares, Y. Huttel, *Nanoscale* **2017**, 9, 6463.
- [34] D. S. B. Everitt, S. Landau, M. Leese, *Cluster Analysis*, Wiley, **2011**.
- [35] V. Estivill-Castro, *SIGKDD Explor.* **2002**, 4, 65.
- [36] S. P. Lloyd, *IEEE Trans. Inf. Theory* **1982**, 28, 129.
- [37] A. K. Jain, *Pattern Recognit. Lett.* **2010**, 31, 651.



Dr. Guillermo Bárcena-González is a recognized expert in image processing and pattern recognition applied to electron microscopy imaging. Assistant Professor of the Computer Engineering Department at the University of Cádiz at Spain (UCA). He received his PhD in Computer Engineering from the University of Cadiz, Spain. His research spans processing images, patter

	recognition, super-resolution and artificial vision applied to electron microscopy images. Member of the research group 'Intelligent Computing Systems' since 2012. He has published high impact articles in prestigious journals and has designed commercial software for companies involved in electron microscopy.
	Andrei Hernández-Robles is a doctoral candidate in Physics at the University of Texas at San Antonio (UTSA). His research includes topics in materials science such as the analysis of defects in nanostructured materials, design and synthesis of nanomaterials, analysis of crystalline materials properties, advanced electron microscopy techniques based on electron diffraction methods, and image processing algorithms based on machine learning to the evolution of dynamic systems in transmission electron microscopy.
	Dr. Lidia Martínez received her European PhD from the Universidad Complutense de Madrid, Spain, focusing her studies in materials science and technology. Guest researcher at Université de La Rochelle, France. She is distinguished reseacher at the Instituto de Ciencia de Materiales de Madrid (ICMM), from the Consejo Superior de

	<p>Investigaciones Científicas (CSIC). Her research is focused in low-dimensional advanced materials, mainly on the study of nanoparticles, which includes their manufacture using gas aggregation sources and their characterization using various techniques such as X-ray photoemission spectroscopy (XPS) or atomic force microscopy (AFM).</p>
	<p>Dr. Yves Huttel received his Ph.D. from the University of Paris-Sud, Orsay, France. Then he worked at the Synchrotron LURE, France, at the University of Paris-Sud, France, and at the Instituto de Ciencia de Materiales de Madrid (ICMM) that belongs to the Consejo Superior de Investigaciones Científicas (CSIC), Spain. He was also a postdoctoral researcher at the Synchrotron of Daresbury Laboratory, UK. Since 2007, he is permanent Scientist at the ICMM where he leads the Low-Dimensional Advanced Materials Group. His research focuses on low-dimensional systems including surfaces, interfaces and nanoparticles, as well as XMCD, XPS and nanomagnetism.</p>



Dr. Álvaro Mayoral obtained his PhD degree at the University of Birmingham in Materials Science. He then worked for two years at UTSA on the study of metal nanoparticles by electron microscopy. He currently works at the Spanish Research Council developing advanced functional materials based on ordered porous solids (zeolites, MOFs and mesoporous silica) and metal nanoparticles through the atomic understanding by transmission electron microscopy. Additionally, he holds a position as visiting scientist at ShanghaiTech University. He has published over 170 SCI articles, several book chapters and being editor of one book.



Pedro L. Galindo is Full Professor of the “Computer Science and Engineering” department and leader of the “Intelligent Systems” research group at the University of Cadiz. His research interests are applications of Artificial Intelligence and advanced Image Processing techniques in real problems, including extraction of quantitative information from electron microscopy images at atomic level for research purposes. He has led several 4.0 industry projects with companies including Airbus (leader in the aerospace industry), Navantia (largest shipbuilding industry in Spain) or Acerinox (largest stainless steel


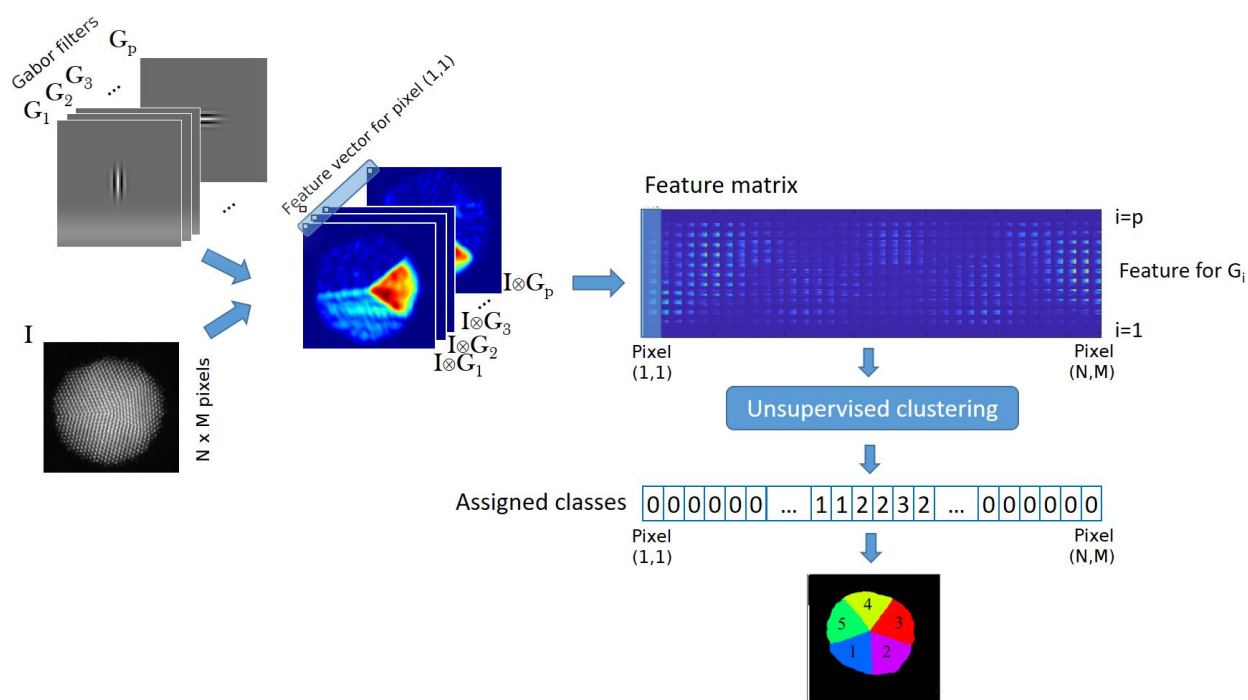
	producer company in the world) in different fields (Robotics, Artificial Vision and Big Data).
	<p>Dr. Arturo Ponce is a recognized expert in materials science and electron microscopist. Professor and Assistant Department Chair of the Department of Physics and Astronomy at the University of Texas at San Antonio (UTSA). He received his PhD in Materials Science from the University of Cadiz, Spain and worked as postdoctoral researcher at UNAM, Mexico and CNRS, France. His research spans the theory and experimental aspects of the atomic structure, physical properties, and manipulation of materials at the nanoscale based on the electron-matter interaction phenomena including electron diffraction, electron holography and in situ microscopy. He leads the Structure Physics and Electron Microscopy group at UTSA.</p>

Table of contents

1. Introduction	2
1.1 Gabor filters.....	3
2. Results and discussions	7
3. Conclusions	13
4. Methods	14

4.1 Production of nanoparticles.....	14
4.2 Electron microscopy.....	14
4.3 Feature Extraction	14
4.4 Unsupervised learning.....	14
4.4.1 Dependence of the segmentation on the number of clusters.....	17

ToC Figure



Supporting Information

Unsupervised learning for the segmentation of small crystalline particles at the atomic level

Guillermo Bárcena-González^{1,+}, Andrei Hernández-Robles^{2,+}, Álvaro Mayoral^{3,4}, Lidia Martínez⁵, Yves Huttel⁵, Pedro L. Galindo¹, Arturo Ponce^{2*}

¹Department of Computer Science and Engineering, University of Cádiz, Puerto Real 11510, Spain

²Department of Physics and Astronomy, University of Texas at San Antonio, San Antonio, Texas 78249, USA.

³Instituto de Nanociencia y Materiales de Aragón (INMA), CSIC-Universidad de Zaragoza, Zaragoza 50009, Spain.

⁴Advanced Microscopy Laboratory (LMA), University of Zaragoza, 50018, Zaragoza Spain. ⁵Instituto de Ciencia de Materiales de Madrid (ICMM-CSIC), 28049, Madrid, Spain.

⁺These authors contributed equally to this work

*Corresponding author

I. Gabor filter parameters

Gabor filters have two main characteristics to extract specific observations from the input material, the wavelength, and the orientation. The first parameter regulates the girth of the applied filter, in terms of an input image, this parameter targets features in function of the given width and in a certain orientation. The latter parameter, the orientation, governs the rotation of the filter in the axis normal to the image, this parameter is crucial to detect misoriented features. **Figure S1** displays both parameters, the sequence a-c) are representative of the increment in wavelength values, 5, 10 and 15 pixels per cycle, which is noticeable in the size of the bandpass. Figure S1 d-f) demonstrate the rotation of the filter in different angles: 0, 45 and 90 ° with respect to the vertical axis and counter-clockwise.

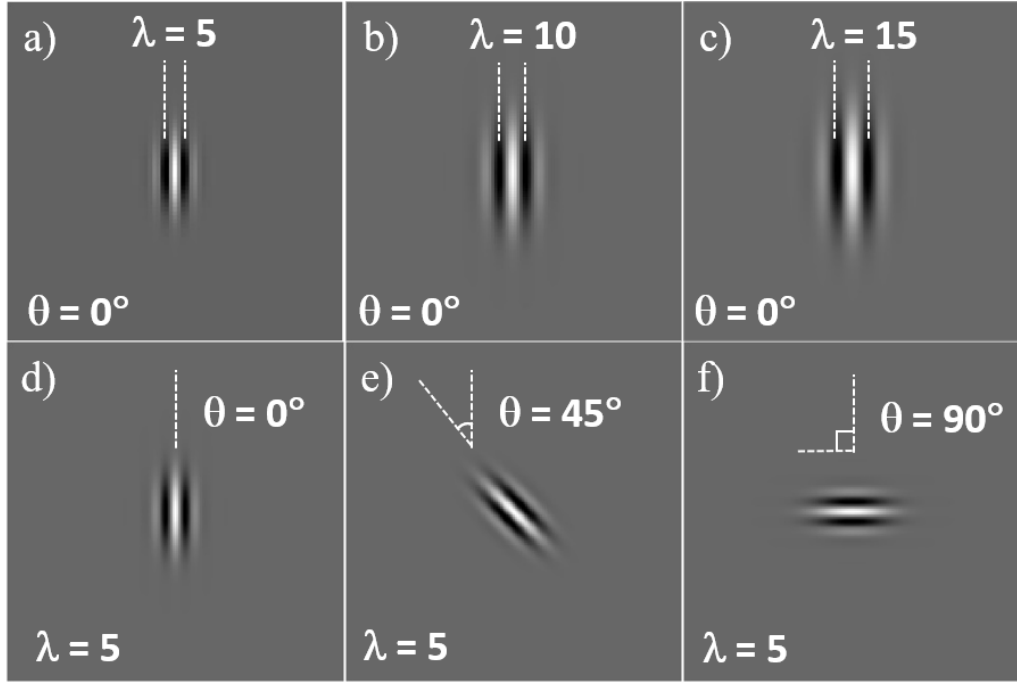


Figure S1. Visualisation of the real part of a Gabor filter for different wavelengths (λ) a) 5, b) 10 and c) 15 and orientations (θ) of d) 0° , e) 45° and f) 90° .

II. K-means algorithm

One of the tasks we can perform on a given data set is to find groups of data which are similar to one another, usually called clusters in an unsupervised way, that is, having no labels for each data point. Therefore, clustering algorithms categorize a set of items into groups of similarity. The clustering method used in this paper is the K-Means^{R1-R3} using the Euclidean distance as the similarity metric, as it is very simple and, by far, the most popular approach for many purposes. It may be described as follows:

Let K to be the desired number of clusters, and a dataset of N points, each described using M features ($x_i \in \mathbb{R}^M$, $i=1..N$)

1. Define randomly K initial centroids (usually, these are randomly chosen from the given data set)
2. Repeat until end-condition meets
 - a. Find the closest centroid to each item, assigning the item to this centroid
 - b. Recalculate the centroids as the average point of all data belonging to each centroid

In method presented herein, N corresponds to the number of pixels in the analyzed image, and M corresponds to the number of Gabor features for each pixel, directly dependent on the number of orientations and spacings used for filtering. At the end, each pixel is classified into one of K clusters depending on their similarity to each other, depending on their Gabor features. One of the main drawbacks of the K-means algorithm is that it does not guarantee convergence to a global optimum. The result may depend on the initial centroids randomly chosen. As the algorithm is usually very fast, it is common to run it multiple times with different initializations. In our experiments, convergence was achieved without problems in all cases.

K-means MATLAB code

The function assumes each data point is stored in a row. Therefore, data is expected to have N rows and M columns, and K is an integer greater than 1

```
function centroids=kmeans(data,K)
% KMEANS – K-means algorithm
%
% data : NxM data matrix of N points with M characteristics
% K : desired number of centroids
% centroids : KxM matrix of K points with M characteristics

% 1. Choose random initial centroids
choice = randperm(size(data,1),K);
centroids = data(choice,:);
oldcentroids = zeros(size(centroids));

% 2. Loop
it = 1;
while (sumsqr(oldcentroids-centroids)>1e-6) && (it<30)

    oldcentroids = centroids;

    % 2a. Calculate closest centroid to each data point
    for i=1:K
        d(:,i) = pdist2(data,centroids(i,:));
    end
    [~,class]=min(d,[],2);

    % 2b. Recalculate centroids
    for i=1:K
        centroids(i,:)=mean(data(class==i,:));
    end

    % Increase loop index
    it = it + 1;
end
```

III. Analysis of a decahedra nanoparticle in TEM mode

The segmentation process has proven to perform optimally in STEM conditions, the reduction of background noise and the slight improvement of the resolution due the nature of this mode smooths the convergence of the algorithm. However, the evaluation of the performance of the segmentation process in TEM mode images was performed for similar nanostructures, the particle segmentation shown in **Figure S2** display the original image, a cropped version to haste the process which was the same area represented in Figure S2 b. Finally, in Figure S2 c the colourization of the previous image is done, it is important to note that the algorithm is capable of discern the particle from the background even in the presence of additional noise due the carbon film where particles are suspended. This process was stopped at K=6.

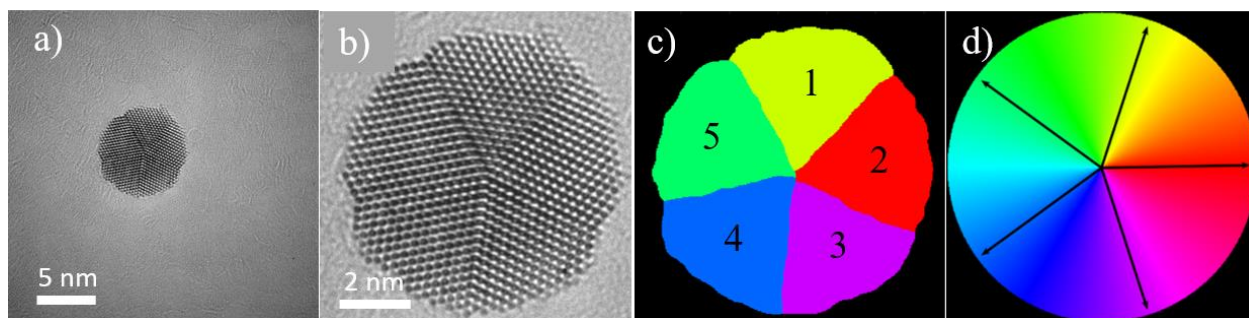


Figure S2. Segmentation of a single decahedral particle in a TEM image. a) complete field view of the micrograph containing the nanoparticle. b) segregation of the main facets, and the background, of the nanoparticle delimited by line due the detection of 6 suitable clusters. c) Colorization of the clusters detected in b). d) colour wheel representing the orientation of the crystallites observed in the specimen, the arrows are spaced by 72° representing the even separation between the tetrahedral substructures.

S4. Segmentation of a complex nanostructure.

In order to evaluate the algorithm in non-ordinary conditions, a STEM image was evaluated, this image (**Figure S3 a**) contains several nanoparticles merged into a single structure, for most of the parts along the formation, the decahedral build seems to be predominant, with a few regions where other tetrahedrons are present as secondary defects. The image was cropped to the region delimited in the yellow-dotted square, after the segmentation method was applied, the particle was subdivided by the principal facets in the particle, at $K=7$ most of the attributes are observed, and the algorithm was stopped at $k=16$, to enhance features on smaller particles. The bigger facets in the particle were consistent with the penta-twinned particle, around the lower part of this region a couple of facets were detected, these facets were identified as those upper regions present in the decahedral particle, making these facets identically oriented.

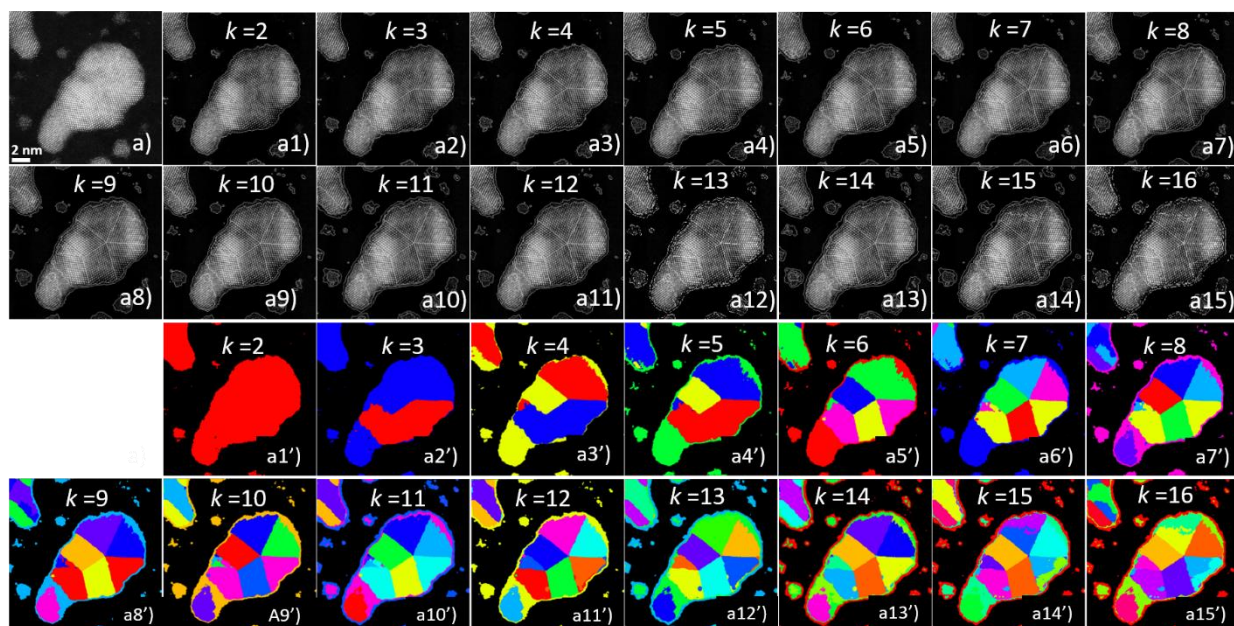


Figure S3. Segmentation process of merged nanoparticles. a) complete field of view of the subject. a1-15) assignation of observations to clusters among the sample for $k=2-16$. a1'-15') colourisation of the observations at $k=2-16$.

References

- [R1] Lloyd, S. P. *IEEE Trans. Inf. Theory* **1982**, 28, 129.
- [R2] MacQueen, J. In *Proceedings of the fifth Berkeley Symposium on Mathematical Statistics and Probability*, Vol. 5.1; **1967**; pp. 281-297.
- [R3] Jin Xin and Han, J. In *Encyclopedia of Machine Learning*; Sammut Claude and Webb, G. I., Ed.; Springer US: Boston, MA, **2010**; pp 563–564.

